Growth of Nitrogen-Containing Carbon Nanofibers

Honors Thesis for Graduation with Distinction
Submitted May 2006
By Eugenia Wang

The Ohio State University
Department of Chemical and Biomolecular Engineering
140 West 19th Avenue
Columbus, OH 43210

Honors Committee:
Professor Umit S. Ozkan, Advisor
Professor David Tomasko

Acknowledgements

I would like to sincerely thank everyone who has helped me along the way with this project. First, I'd like to thank my family for always encouraging me to take on new and challenging endeavors. I would also like to thank the Heterogeneous Catalysis Research Group for providing such a welcoming atmosphere. The group's willingness to help is something every undergraduate student starting out in research could hope to get and more. I would like to extend a special thanks to Dr. Umit Ozkan and Paul Matter for their invaluable support, direction, and confidence in my ability to carry out this project. Additionally, I'd like to thank my boyfriend for always making sure I took care of my health, even through the busiest and most stressful times. Lastly, I wanted to say that I appreciate my girls for being there to help me relax when I needed to the most. This experience has truly been a great one!

Abstract

Nitrogen-containing nanofibers are lightweight, can be functionalized for electrical and thermal conductivity, and can be useful for mechanical reinforcement, which are properties that can be used for many practical applications. However, different metals and supports affect the structure of the carbon nanofibers that are formed. Different combinations of supports (MgO and SiO_2) and metals (Co, Fe, Ni) were used as catalytic precursors to grow nitrogen-containing carbon nanofibers via acetonitrile decomposition. The products were analyzed using thermal gravimetric analysis (TGA), BET surface area/pore volume analysis (BET standing for Brunauer, Emmet, and Teller, the people who developed the technique for calculating surface area), temperature programmed acetonitrile pyrolysis (TPAP) analysis, temperature programmed oxidation (TPO) analysis, and transmission electron miscopy (TEM). MgO supports were easier to purify making it more favorable than SiO_2. Co containing catalysts seemed to produce nanofibers with the highest nitrogen content, with Fe and Ni to follow. Fe and Co loaded catalysts yielded products with a stacked cup shape, which has easily functionalized edge planes. Diameter size distributions of the fibers grown seemed to be independent of the catalytic precursor; however, Co containing catalysts produced fibers with more uniform sizes. Following this study, fibers can now be produced with respect to specifications in shape, size, and nitrogen content.

Table of Contents

List of Figures

List of Tables

1) Introduction

1.1) Overview

Carbon nanofibers have been introduced to the research world as a promising means to improve existing technologies as well as to aid in the creation of new ones. Different catalyst compositions as well as growth atmospheres will result in different types of carbon at the nano-level. Studying the conditions that nitrogen-containing carbon fibers are made as well as inducible properties like conductivity and mechanical reinforcement, will allow them to continue to be a frontrunner for many practical applications. For example, the unique chemical and physical properties associated with carbon nanofibers can be put to good use in diverse applications, such as catalyst supports, polymer reinforcement agents, fuel cell electrodes, adsorbents, and energy storage [1].

1.2) Carbon nanofiber production and resulting physical properties

Experiments have been conducted on various ways to produce carbon nanofibers. Different catalysts studied include metals catalysts, metal supported sol-gel catalysts, metal supported graphitic catalysts, polymers, and floating catalysts. The use of inexpensive transition metals, such as nickel, iron, and cobalt, in catalysts were approached with high interest. Commonly studied feed conditions include the decomposition of ethylene, carbon monoxide, and acetonitrile. Differing combinations of these growth atmospheres produced differently shaped carbon nanofibers. Commonly seen structures are multi-walled nano-tubes (MWNT's), as shown in Figure 1, which are tubular with carbon planes that run lengthwise of the fiber axis [2, 3, 4**]**. This fiber shape allows them to be useful in nano-wires or composite materials because of their high

conductivity and mechanical strength in the axial direction. Another typically formed carbon nanofiber structure is stacked platelet carbon, which has graphite planes aligned perpendicularly to the fiber axis. The edges of the planes, which can be easily functionalized, are exposed [4]. See Figure 2 for an image. MWNTs are mechanically stronger and conductive down the axis, while stacked platelet carbon provides better reactivity. Additionally, many hybrid structures between the two exist. The herringbone structure, as depicted in Figure 3 is a prime example of a hybrid structure [2, 4, 5, 6]. Again, these structures have a large number of edge sites, which makes them useful for catalytic activity. Another aspect, besides merely the structure of the carbon planes, is the appearance of a carbon plane itself. Figure 4 depicts a two-dimensional representation of a single carbon plane.

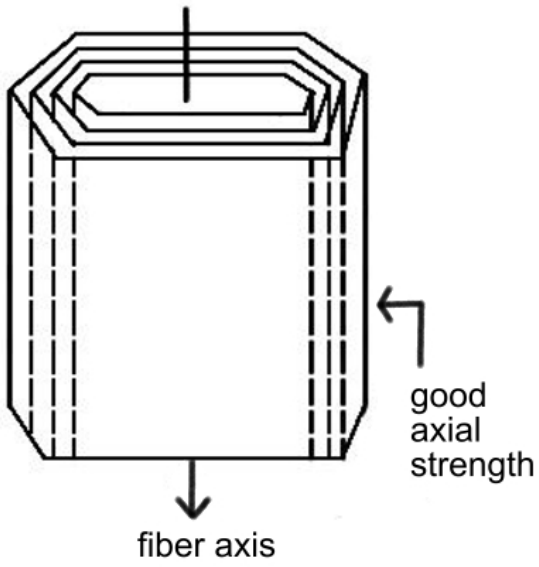

Figure 1: Depiction of MWNTs.

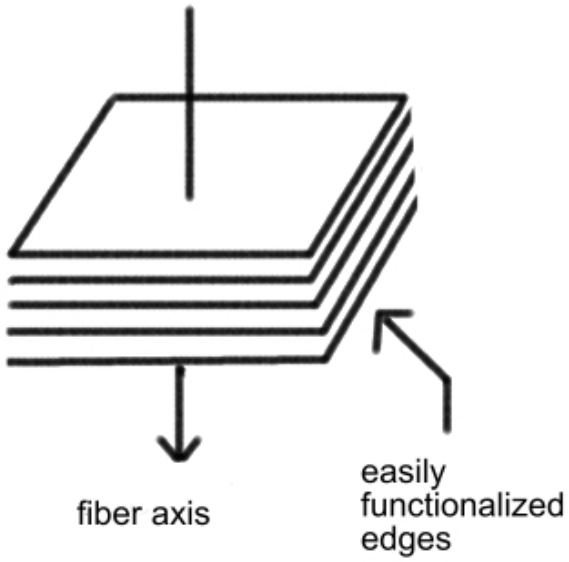

Figure 2: Depiction of stacked platelet carbon.

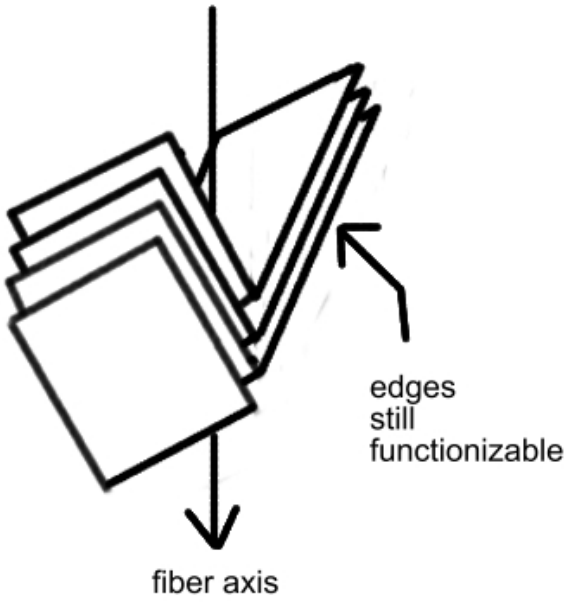

Figure 3: Depiction of stacked herringbone carbon

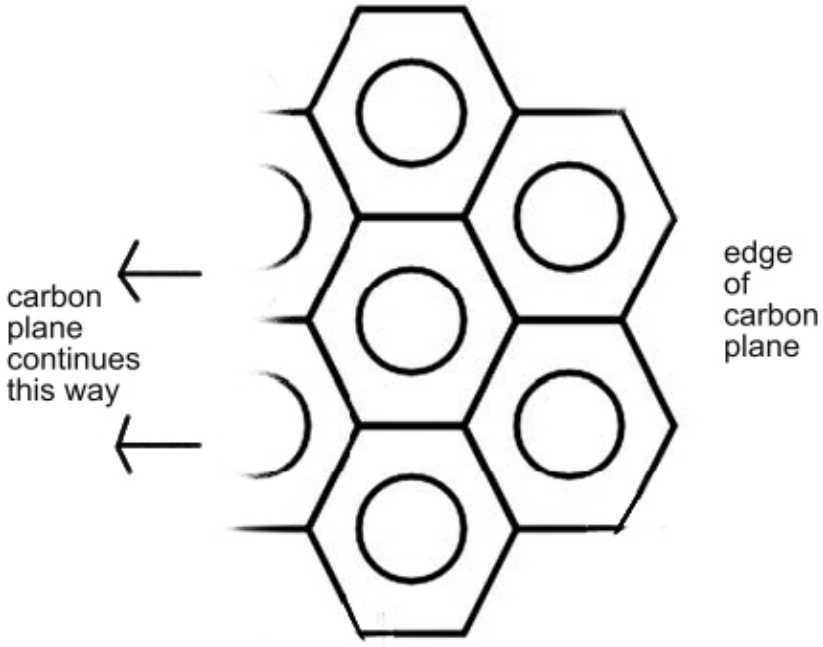

Figure 4. Carbon plane.

1.3) Nitrogen-containing nanofiber production

Because of the potential usefulness that nitrogen-containing carbon fibers have, studies have already been conducted on how to produce them from their catalyst precursors. Problems, however, exist with some of the most commonly used catalyst precursors. Fibers can be formed from pure metal particles; however, to obtain smaller fibers with a narrow distribution, it is better to disperse the metal catalyst on an inorganic support. Previously, our group prepared nitrogen-containing carbon fibers from a sol-gel alumina support [3]. For the sol-gel technique, an alkoxide is used to form a metal oxide. The metal oxide is then used as a support for the metal particles that the fibers grow from. Alumina, a support that has been studied in depth, needs to be removed from the resulting carbon nanofibers using a tedious HF wash. Alternative supports, such as silica or

magnesia, can be more easily removed using KOH or HCl washes. As previously mentioned, an alternative procedure can be used, synthesis of the fibers using a floating catalyst method. It has been discovered that use of such a method with ferrocene and cobaltocene as catalytic precursors successfully produces herringbone-stacked carbon nanofibers at a selectivity close to 100% [6]. The main advantage of developing this method is that a floating catalyst process has no support to remove. In addition to that, it is possible to carry out the process continuously. Not only does this procedure have the potential to eliminate the problem of low product yields but it also reduces the number of variables (since it does not require a support), making it easier to analyze resulting characteristics with respect to the others. By applying different fiber growth conditions, analysis of resulting products can help the discovery of quantity optimization as well as new properties.

1.4) Applications for nitrogen-containing carbon nanofibers

As previously mentioned, nitrogen-containing carbon nanofibers have chemical and physical attributes that are useful for many practical applications. One of the aforementioned uses was as an adsorbent. For the case of water purification, platelet-type structured carbon nanofibers are useful. The highly ordered, nearly crystalline structure exhibits superior selective adsorption properties with respect to removal of alcohols from aqueous media over active carbons [7]. Another useful property that nitrogen-containing carbon nanofibers display is electrical conductivity. An important physical characteristic that promotes this behavior is the ordered structure of the nanotubes. Additionally, the geometrical structure of the carbon nanofibers affected their properties; these nanotubes can either act as metals or semiconductors depending on the

relative position of nitrogen and carbon atoms [8]. Because nitrogen-containing carbon nanofibers have this property, they can be used in nanosized electronic devices in the future.

Although nitrogen-containing carbon nanofibers have many possible uses, none of them has induced as much excitement as the possibility of their use in fuel cells. Fuel cells offer a cleaner, potentially more efficient source of energy than traditional internal combustion engines and other energy-conversion devices. Currently proton-exchange membrane (PEM) fuel cells are under consideration in use for mobile applications, because their low operating temperature allows for quick start-up [3]. Listed below are the individual half cell reactions as well as the net reaction that a fuel cell undergoes.

$$2H_2 \rightarrow 4H^+ + 4e^- \qquad \text{(anode reaction)}$$

$$O_2 + 4H^+ + 4e^- \rightarrow 2H_2O \qquad \text{(cathode reaction)}$$

$$2H_2 + O_2 \rightarrow 2H_2O \qquad \text{(net reaction)}$$

The currently used catalyst for the cathode reaction, platinum, is expensive and is relatively slow, making it a bottleneck for the commercialization of fuel cells. However, nitrogen-containing carbon nanofibers have shown promise for the oxygen reduction reaction (ORR), which is the cathode half-cell reaction. First, experimental results in testing nitrogen-doped and non-nitrogen doped catalysts gave markedly different results. The incorporation of nitrogen into the carbon nanofibers resulted in more facile adsorption of oxygen and greater activity for heterogeneous hydroperoxide decomposition [5]. By further studying characteristics of these activated carbon materials that have their surfaces functionalized with nitrogen, correlations can be made from those physical properties to catalytic properties. For example, a link between the activity in

H_2O_2 decomposition and that in O_2 reduction for several of carbon-based contacts used as catalyst and electrode materials has already been observed [13]. Additionally, a conjunction between catalytic activity increased and basicity has been shown. An explanation for this would be increased pyridinic nitrogen, a basic group, which is found in more active samples; however, pyridinic nitrogen itself may merely be a marker for edge plane exposure rather than an active site for ORR [3]. Because of correlations between pyridinic nitrogen and exposed edge planes and high ORR activity, nitrogen-containing carbon nanofibers are a good starting point for the design of a carbon-based oxygen cathode.

1.5) Project Plan

The procedure of growing the fibers from a catalyst was approximately the same for every sample. The process used from catalyst preparation to fiber purification, is summarized in Figure 5. Additionally, Figure 5 denotes the characterization tests done on the fibers and during which stage it was completed. Each support had its pore volume determined first. After the metal/support combination was chosen, the catalytic precursor was formed via incipient wetness treatment. Thermal gravimetric analysis (TGA) and a temperature programmed acetonitrile pyrolysis (TPAP) was done in order to determine weight loss of the catalyst and byproducts formed, respectively. The precursor was then subjected to pyrolysis. Afterwards, surface area and pore volume was analyzed. The fibers were washed, and then the surface area and pore volume analysis was repeated for comparison purposes. Temperature programmed oxidation (TPO) helped characterize the composition of the final product, and transmission electron microscopy (TEM) was used to analyze the structures of nitrogen-containing nanofibers that were formed.

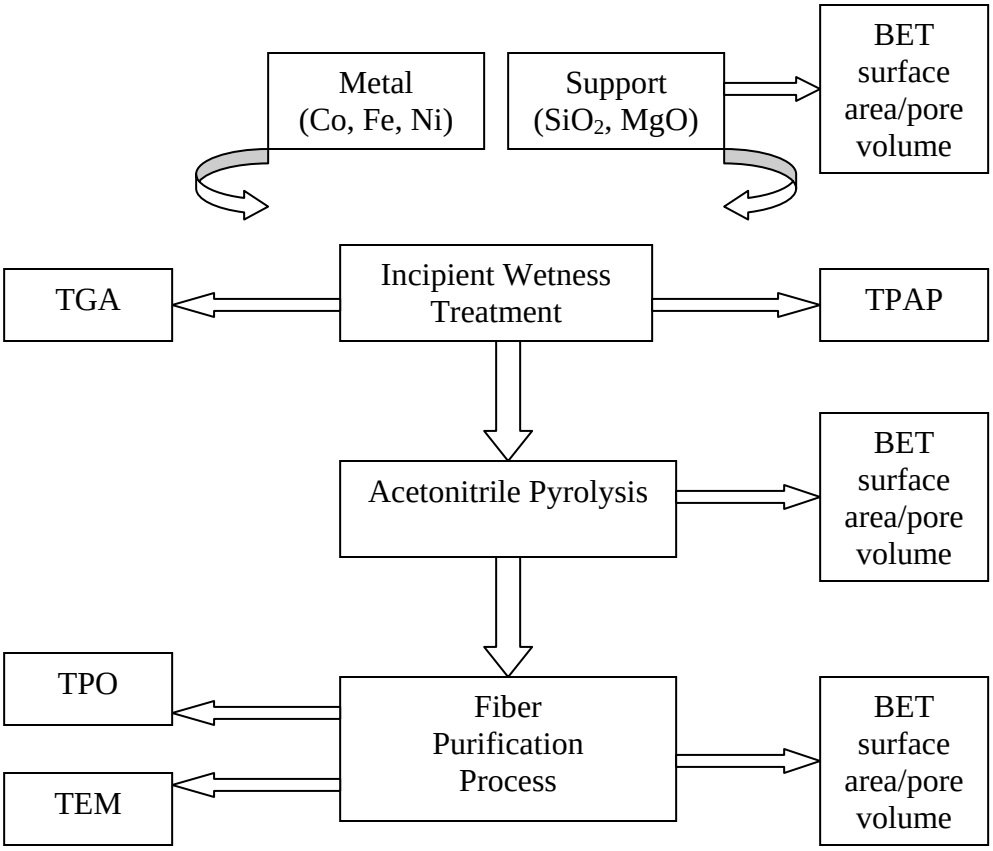

Figure 5. Fiber preparation and characterization process.

1.6) Importance of continued study

Continued research in nitrogen-containing carbon nanofibers, especially where fuel cells are concerned, is aligned with public interest. As fossil fuels, the traditional source of energy, increase in price due to dwindling supplies and increasing demands, making fuel cells a viable alternative becomes increasingly important.

2) Literature Review

Nanotechnology has been praised as having the possibility to revolutionize technology. Carbon nanofibers can be grown from different catalytic precursors including metals catalysts, metal supported catalysts, polymers, and floating catalysts. Additionally, different growth atmospheres have produced differently shaped structures on the nano-level. Further studies have been done on nitrogen-containing carbon nanofibers in particular, which have shown promise in having uses for many applications, such as fuel cells, hydrogen storage materials, composite additives for aerospace materials, and electronic devices.

Rodriguez's group studied the catalytic engineering of carbon nanostructures citing the procedure of decomposing carbon-containing gases over certain metal surfaces [4]. Not only did they study a copper-iron bimetallic powder, but they also studied silica-supported iron catalysts. It was shown afterwards that the metal catalysts as well as feed composition had a tremendous impact controlling the growth characteristics of carbon nanofibers. Additionally, the width of the nanofiber formed was also found to be directly related to the pretreatment and preparation of the catalyst. Iron based catalysts in conjunction with their interaction with CO/H_2 produced carbon nanofibers that were the shape of graphite platelets stacked perpendicular to the fiber axis, while the reaction of CO/C_2H_4 over silica supported iron particles yielded graphite platelets stacked in a direction parallel to the fiber axis. The carbon nanofibers created by decomposition of ethylene/hydrogen over the iron-copper bimetallic catalyst, yet another growth atmosphere, yielded differently shaped carbon nanofibers than the previous two. This time a herringbone stacking arrangement was observed [4]. Refer back to Figure 1,

Figure 2, and Figure 3 for examples of tubular stacked, platelet stacked, and herringbone stacked carbon nanofibers, respectively. Feed condition, however, was not the only aspect that affected the structure of the nanofibers; the metal and the support chosen also caused differently structured carbon nanofibers to form. One study examined the decomposition of ethylene using three metals (Fe, Ni, and Co) on three different supports (silica, graphite, and platelet graphite nanofibers (GNF)). Fe/silica catalysts yielded uniformly sized tubular structured nanofibers [2]. Moreover, the carbon seemed to have grown in an extrusion mode, meaning that the iron stayed attached to the support surface. In contrast, Fe/graphite and Fe/GNF catalysts produced structures that indicated that the Fe particle was lifted away from the support. Co systems yielded different structures altogether. The Co/silica catalyst had low yields of short tubular nanofibers. However, graphite supported catalysts exhibited two types of nanofibers: (1) a jagged, stacked cup structure with no well-defined axis and (2) uniform tubular structures. Nickel-supported catalysts yielded the largest amount of solid carbon, but did not have smooth profiles. The carbon nanofibers grown were herringbone shaped [2]. Different catalysts and growth atmospheres affected the synthesis of the carbon nanofibers generating structures that exhibited different formations. Additionally, they all possessed relatively high active surface areas with a large number of carbon edge sites [4]. For catalysis study, this is a promising result.

The sol-gel method has been to prepare supports for metal catalysts. Its advantages include having well-defined pore size distribution. Additionally, it is pure and homogeneous, and it has the ability to form large surface area materials at low temperatures [9]. Preparation includes precipitation of one or more of the metal soluble

salts using base addition to precipitate the metal oxide gels. Later, impregnation of the support is accomplished when the metal to be deposited on the support is put in contact with it. Existing supports made by this process include silica, alumina, magnesia, titania, and zirconia. These sol-gel methods have produced catalytic activities and selectivities comparable to catalysts prepared by traditional methods. Potential applications of catalysts prepared by sol-gel processing are tied to their high thermal stability, their resistance to deactivation, and the flexibility in porosity, surface area, and pore diameter control. Gonzalez's group studied the sol-gel process in depth, citing additional studies needing to be conducted on dispersed inexpensive transition metals, such as Cu, Fe, and Co on these supports [9]. Another group studied nitrogen doping of the carbon nanofibers using a catalyst of Co/SiO_2, one of the transition metal induced sol-gel catalysts previously mentioned. The carbon nanotubes were grown by decomposing acetonitrile on the catalyst via heat treatment. This action introduces basic sites, which later become active sites for the catalyst [10]. Results showed mainly two types of nitrogen-carbon bonds existed. The pyridinic type is located at the tube's edge, while the quaternary type is located in the graphene layers with temperature treatment affecting the amount of nitrogen at the surface. Afterwards, nitrogen-containing nanofibers were studied in more detail in order to understand the physio-chemical properties of the materials and their catalytic activity.

Polyacrylonitrile (PAN) has been largely used to create carbon fibers at high yields [11]. Accordingly, experiments using the polymer as a precursor for making carbon nanofibers were conducted. When mixed with a high-area carbon and cobalt or iron salts and then heat treated, PAN based catalysts became very promising, especially

in the field of O_2 reduction [12]. The Gupta group proposed heat treatment in conjunction with the macrocycle pyrrole ring is the source of the catalytic activity that has been found. With this model, the modified carbon surface on which transition metal ions are adsorbed interacts with the residual nitrogen derived from the heat-treated macrcycoles. These nitrogen-containing carbon nanofibers were then tested in order to check their affect on electrical conductivity. Results from the group showed that cobalt-based materials were found to be more active by showing promising performance for O_2 reduction in alkaline and acid electrolytes [12]. Again, these nitrogen-containing nanofibers were found to have many uses, this time being their catalytic activity, which has promising uses in fuel cells.

More recently, synthesis of carbon nanofibers using a floating catalyst has been examined. Singh's group discovered that herringbone-stacked carbon nanofibers with near 100% selectivity could be produced using a cobaltocene precursor in the presence of thiophene [6]. (See Figure 3 for a picture of herringbone-stacked carbon.) They also looked at a ferrocene catalyst in order to synthesize herringbone carbon nanofibers, but the selectivity was not nearly as high. Additionally, the group showed the affect of ethylene and thiophene on the system. Contrary to original belief, acetylene was not the carbon supplier. Instead, thiophene, once thought to be merely a promoter, was the carbon supplier for the system [6]. Maldonado and Stevenson also studied floating catalyst growth of carbon nanofibers. These nanofibers were doped with nitrogen using purge and feed gases of ferrocene in xylene or pyridine [5]. The N-doped carbon nanofibers were seen to have a stacked cup type structure and to have more unstructured edges. Additionally, electrochemical studies of oxygen reduction using these fibers

demonstrated better catalytic activity, which is a property that can be useful in sensors, batteries, and fuel cell electrodes. Laboratory work has also been done on nitrogen-containing carbons that were prepared by pyrolysis of acetonitrile over a series of Vulcan carbon and metal-doped Vulcan carbon supports [3]. Similarly, to the results that Maldonado and Stevenson had seen in their floating catalyst study, iron doped samples resulted in the formation of carbon nanostructures with high edge plane exposure [3, 5]. These catalysts, tested for their activity in the oxygen reduction reaction, showed promising results with rising activity being related to rising amount of pyridinic-nitrogen.

Many groups that have studied nitrogen-containing nanofibers have mentioned a potential use for fuel cell applications. In one particular study, surface properties of activated carbon materials that were modified with oxygen and/or nitrogen atoms on their surfaces were examined. Special attention was paid to their catalytic properties in decomposing hydrogen peroxide and in electrochemically reducing O_2 in aqueous electrolytes. Because catalytic activity for O_2 reduction was found to correspond with that for HO_2^- decomposition, the selection of active catalysts for the heterogeneous decomposition of HO_2^- is a good starting point for the design of a carbon-based oxygen cathode [13]. Additionally, nitrogen-containing carbon nanofibers have electronic properties, which have been tested for as well [8]. Huang's group specifically studied the geometrical and electronic properties of nitrogen-containing carbon nanotubes. The result was that these nanotubes could act as metals or semiconductors depending on the relative position of nitrogen and carbon atoms. Moreover, the relative position of nitrogen and carbon atoms not only affected electronic properties, but also stability. The most stable non-metallic tubes are narrow energy gap semiconductors, while the metallic

tubes have two overlapped partially filled bands [8]. This study yielded that nitrogen-containing nanofibers have potential in not only fuel cell applications, but also for nanosized electronic devices in the future.

3. Experimental Methods

3.1 Catalyst Preparation

Nitrogen-containing carbon fibers were prepared using a catalyst of metal, Ni, Co, or Fe, supported on a metal oxide, either SiO_2 or MgO. The SiO_2, purchased from Alfa Aesar, had a surface area of 215 m^2/g and was used without further treatment. Two types of MgO support were used. The first MgO support had a surface area of 55 m^2/g, and was used as received from Leco Co. The second type of MgO, a "nanopowder," was used as received from Sigma-Aldrich and had a surface area of 150 m^2/g. The supports were impregnated by incipient wetness with an aqueous solution of the metal acetate salt. A concentration of the acetate solution was chosen such that the final metal loading would be 2-wt% (unless otherwise noted), and the total volume of water used would be equivalent to the total volume of the support pores. (In situations where the acetate salt was not able to be dissolved within the amount of water that it took to fill the pores, the salt was dissolved with the appropriate amount of water. The incipient wetness method was used several of times. An amount of metal acetate solution equal to that of the total volume of the support pores was added; the catalyst was then dried. This procedure was repeated until all of the metal acetate solution had been put on the support.) Afterwards, the precursor was dried at 100^oC overnight. Thermal gravimetric analysis (TGA) was used to determine the weight loss incurred during temperature ramping in an inert atmosphere to accurately determine the carbon yield after the acetonitrile treatment.

The acetonitrile treatment consisted of decomposing acetonitrile, a process known as pyrolysis, over the catalyst. A total of 2 grams of the catalyst precursor (unless otherwise specified) was used for fiber growth. The precursor was placed in a 6 inch

quartz calcination boat and then sealed inside a quartz tube furnace. The temperature was ramped to the treatment value (550°C or 900°C) at 10°C/min under N_2 flow at 150 sccm. For treatment temperatures of 550°C the metal salt was reduced *in situ* with 5% H_2 in N_2 prior to sending acetonitrile to the precursor, while for temperatures of 900°C, the salt was simply allowed to be reduced by the acetonitrile. The acetonitrile treatments lasted 4 hours for the 550ºC treatment and 2 hours for the 900ºC treatment, using nitrogen saturated (150 sccm) with acetonitrile by means of a room temperature bubbler. After the treatment the temperature was lowered under N_2 flow to room temperature.

3.2) Thermal Gravimetric Analysis (TGA)

TGA determined the weight that the catalytic precursors lost during the temperature ramping process for the acetonitrile treatment. The Perkin-Elmer TGA7 was able to quantitatively measure the change in the mass of a sample. The program started the sample from room temperature and ramped to 850ºC at a rate of 5º/min. The atmosphere that the test was carried out in was N_2 being run through the system at 40 mL/min. Afterwards, the system was allowed to cool back down to room temperature.

3.3) Fiber Purification

Fibers prepared using silica-based supports were purified by subsequent KOH and HCl washes. First, the product from the acetonitrile treatment was refluxed in 1 M KOH, and then washed with distilled water by suction filtration. Afterwards, the remaining fibers were refluxed in 1 M HCl, and then washed with distilled water by suction filtration. The recovered fibers were dried overnight at 100°C. Further analysis was done to determine the composition of the fiber surface after washing, which resulted in less than 2% SiO_2 and 0.1% Cl remaining on the surface.

Fibers prepared using magnesia-based supports were purified using an HCl wash. The product from the acetonitrile treatment was refluxed 1 M HCl, then washed with distilled water by suction filtration. The recovered fibers were dried overnight at 100^{o}C. When further analysis was done, the composition of the fiber surface after washing had no detectable Mg and less than 0.1% Cl.

3.4) BET Surface Area/Pore Volume Measurements

Physisorption analysis of the catalysts was conducted using a Micromeritics ASAP 2010. Liquid nitrogen was used to fill the tube carrying the sample, thus saturating the pores of the sample. Afterwards, the pressure was decreased, which caused the nitrogen to sublime. Naturally, the liquid nitrogen filling the bigger pores would sublime first, thus giving an accurate measurement of the pore diameter distributions of the samples. The program used this information to get the surface area and pore volume at each diameter distribution as well.

This characteristic testing was used on all three of the supports in order to determine the total pore volume in order to complete the incipient wetness procedure, as stated in the catalyst preparation section. Additionally, this analysis was used on samples following the acetonitrile treatment. Both pre-fiber purification and post-fiber purification fibers were tested.

3.5) Temperature Programmed Acetonitrile Pyrolysis (TPAP)

An online Cirrus Mass Spectrometer (MS) was used to analyze the byproducts of acetonitrile decomposition. For these experiments 100 mg of catalyst precursor was placed loosely in a quartz tube in order to avoid plugging during fiber growth. The tube was then placed horizontally in a furnace with the MS sampling the exit stream. The

temperature was ramped from room temperature to 900^{o}C at 10^{o}C/min while flowing He (20 sccm) saturated with acetonitrile at room temperature. The MS scanned for ions between 1 and 100 AMU.

3.6) Temperature Programmed Oxidation (TPO)

Temperature programmed oxidation of samples was carried out in a Setaram TG-DSC 111 with the product stream being analyzed by a Cirrus Mass Spectrometer (MS). Approximately 10 mg of sample was loaded into the TGA, and the temperature was ramped at 5^{o}C/min to 750^{o}C in 10% O_2 in He flowing at 60 sccm (split evenly between the reference and sample side). Both the TG and DSC signals were recorded. The MS was used to follow oxides of nitrogen and carbon that formed from the combustion.

3.7) Transmission Electron Microscopy (TEM)

Transmission electron microscopy was performed with a Philips Tecnai TF20. Samples were supported by lacey-formvar carbon, which was supported by a 200 mesh copper grid. The carbon samples were dispersed with excess ethanol before being deposited of the grid.

4 Results and Discussion

4.1) Thermal Gravimetric Analysis (TGA)

TGA was used in order to determine weight loss of each catalyst during the heat ramping that preceded the acetonitrile treatment. From that, a percent weight loss of the catalyst precursor was calculated, as show in Equation 1. Afterwards, the amount of carbon fibers grown could be calculated. Equation 2 shows how the final weight (wt) gain of the fibers was obtained, while taking weight loss of the precursor into account.

$$\%wt\_loss_{TGA} = (1 - \frac{wt_{final}}{wt_{initial}}) * 100\% \quad (1)$$

$$wt\_gain = (wt_{final} - wt_{empty\_boat}) + \frac{\%wt\_loss_{TGA}(wt_{precursor\&boat} - wt_{empty\_boat})}{(wt_{final} - wt_{empty\_boat})} \quad (2)$$

Table 1 shows the percentage weight gain of each catalyst after undergoing the acetonitrile treatment.

Table 1. Percentage weight gain following pyrolysis.

Catalytic Precursor	Treatment	Weight Gain
SiO_2	550ºC, 4 hours	1.9%
2% Co/SiO_2	550ºC, 4 hours	2.3%
2% Fe/SiO_2	550ºC, 4 hours	3.0%
SiO_2	900ºC, 2 hours	13.0%
2% Co/SiO_2	900ºC, 2 hours	13.6%
5% Co/SiO_2	900ºC, 2 hours	35.8%
10% Co/SiO_2	900ºC, 2 hours	18.8%
2% Fe/SiO_2 (sample 1)	900ºC, 2 hours	18.8%
2% Fe/SiO_2 (sample 2)	900ºC, 2 hours	18.9%
2% Ni/SiO_2	900ºC, 2 hours	6.6%
MgO	900ºC, 2 hours	15.4%
2% Co/MgO	900ºC, 2 hours	17.7%
2% Fe/MgO	900ºC, 2 hours	21.9%
2% Ni/MgO	900ºC, 2 hours	44.2%
MgO (nanopowder)	900ºC, 2 hours	-16.7%
2%Fe/MgO (nanopowder)	900ºC, 2 hours	28.7%

An earlier problem that faced nanofiber growth was the low yield, so TGA was used to obtain the combination of metal and support that resulted with the largest percent weight gain. From Table 1, a couple of outlier points could be spotted. For example, the sample with 5% Co/SiO_2 yielded a larger amount of carbon growth than the 10% Co/SiO_2, which was not expected. Since the carbon nanofibers grow from the metal particles, a higher percentage loading of metal should have resulted in a higher yield of carbon nanofibers. Additionally, the negative weight gain that was reported for the MgO "nanopowder" sample is not possible. Since fibers were grown during the treatment, the weight gain should have yielded a positive number. However, the MgO nanopowder was lightweight and had a fluffy texture. The initial weight of the catalyst could have been easily altered if some of the nanopowder had blown off of the quartz boat and into the quartz tube prior to pyrolysis. This explanation is likely considering the physical properties of the MgO nanopowder and the atmosphere within the calcination tube prior to pyrolysis, which had N_2 flowing through it at 150 sccm. Additionally, observations using the 2% Fe/MgO (nanopowder) sample also backs up this hypothesis. The nanopowder was weighed down after the Fe acetate solution was introduced to it, ridding the powder of its fluffy characteristic. The weight gain results from the 2% Fe/MgO (nanopowder) showed that this catalytic precursor had a relatively high weight gain after pyrolysis. It is also imperative to note that while doing the incipient wetness treatment, MgO nanopowder seemed to escape from the petry dish, which was marked by the visual of dust rising as each drop of the metal acetate solution was added. This would have resulted in the catalyst precursor weighing less than what was initially observed, thus causing the weight gain to be higher than the one reported in Table 1.

Samples ramped to only 550ºC did not grow as many fibers as those that received the decomposition of acetonitrile at 900ºC. Other general trends are that as the percentage of metal loading on the support increased, so did the fiber growth. Additionally, for both MgO and SiO_2, the iron supported catalysts grew more fibers than the cobalt supported catalyst. Nickel, which grew fibers readily when it was supported on MgO, did not have the same affect when supported on SiO_2. Taking into consideration the fact that the MgO support was more easily removed, since it only requires one wash and incidentally left less of the support on the surface, it would most likely be the preferred support to use. Additionally, it was observed that when metal was supported on the MgO nanopowder, the yield of carbon nanofibers following the acetonitrile decomposition was more. When coupled with the TGA, pre-treatment and post-treatment weights of the catalyst could be used to quantify the amount of fibers that grew. Metal supported on MgO seems to be the best catalyst for fiber growth. However, other factors play into finding the catalyst that provides the most desirable characteristics.

4.2) BET Surface Area/Pore Volume Measurements

Physiorption using liquid nitrogen was performed on the supports as well as the product after pyrolysis (both for purified and non-purified fibers). The data collected for the supports determined the total pore volume of the support, which provided key information needed for incipient wetness preparation of the catalytic precursor. Since high surface area and high pore volume measurements are key characteristics for catalysts, testing these physical properties yield information about catalytic properties for the fibers produced from the acetonitrile pyrolysis.

This characterization method was used for fibers produced from the acetonitrile treatment, both pre and post purification. By looking at the samples both before and after washing, the affect of removing the support from the samples can be clearly seen. Figure 6 and Figure 7 represents samples using the SiO_2 support and MgO support, respectively. Figure 6, more specifically, depicts the relationship of pore volume with respect to pore diameter of the 2% Fe/SiO_2 sample. Both before purification (unwashed) and after purification (washed) curves were put on the same graph for comparison purposes. From the graphical data, it can be noted that purification of a SiO_2 based catalyst opened up pore volume at lower pore diameters. However, as the pore diameters rose, the unwashed sample peaked at a much higher value than the washed sample. Figure 7 shows the relationship between the purified and unpurified fibers produced from the 2% Fe/MgO catalyst following the acetonitrile treatment; the washed sample had larger pore volumes at almost every pore diameter distribution. Because of this feature, it can be argued that the washing of the MgO support is more effective. This characteristic leads to greater surface area, which is useful for catalytic purposes.

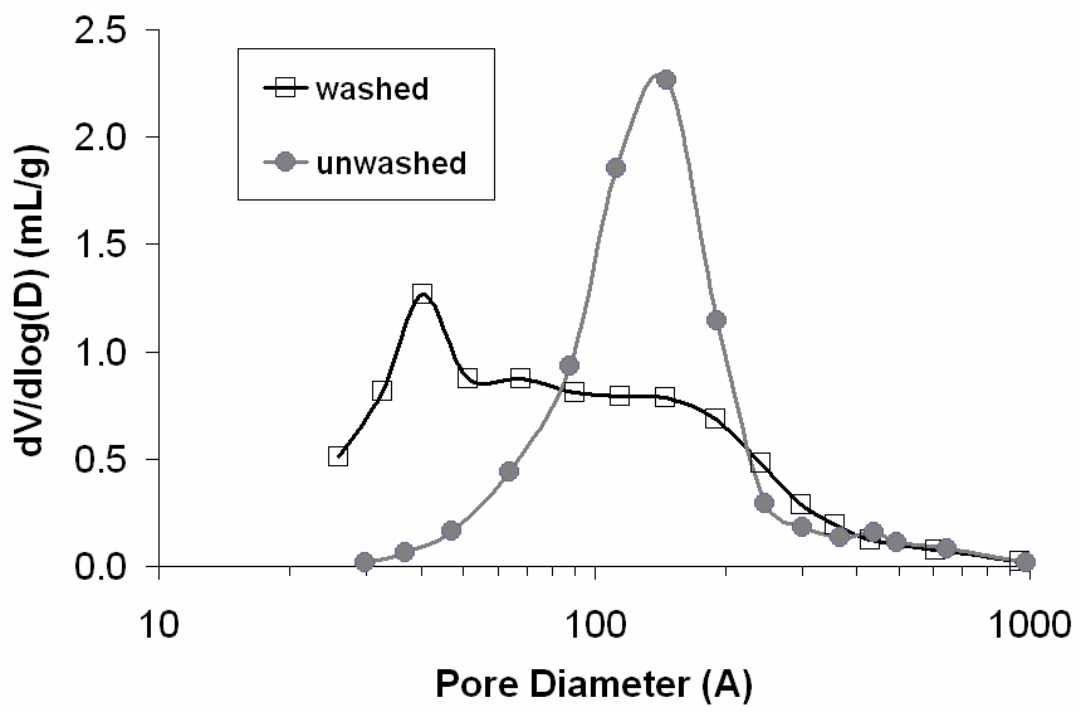

Figure 6. BJH Desorption for 2%Fe/SiO_2

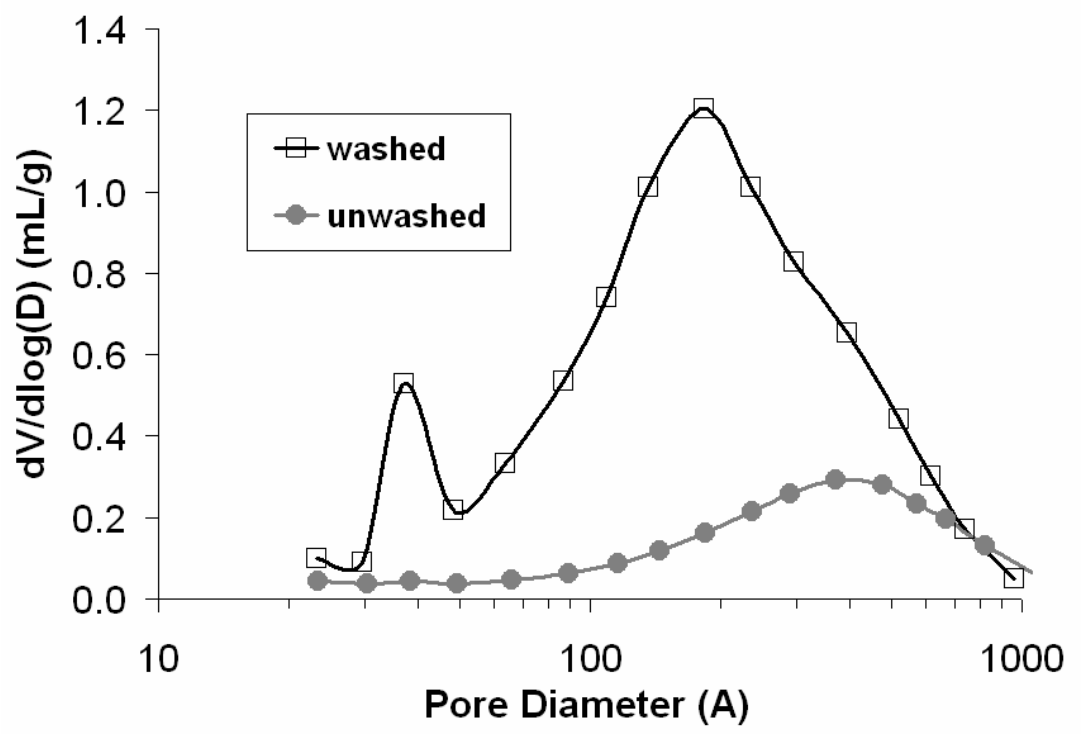

Figure 7. BJH Desorption for 2%Fe/MgO

With comparing Figures 6 and 7, both of the washed curves for the fibers yielded a similar peak at approximately 40 A. One possible explanation for this phenomenon is that the liquid nitrogen somewhat bonded the fibers together. The pressure at which the liquid nitrogen was desorbed, represented by pore diameter measurement, was some sort of critical point that allowed the fibers to once again break apart.

Since high surface area, and thus pore volume, is a generally a characteristic of good catalysts, the physisorption tests were useful in helping determine which combination of metal and support yielded the fibers with the best characteristics. It is important to note that the MgO supports are already favored at this point, seeing as the purification process is easier and seems to be more effective. Table 2 shows the BET surface area and BJH desorption (pore volume) of the purified fibers. As can be seen, 2% Co supported catalysts seemed to have a higher surface area and pore volume than other respective catalysts. In fact, as seen represented by the SiO_2 sample, the surface area and pore volume actually decreased with higher percentages of cobalt on them. This trend would probably follow with other metal supported catalysts, since at a higher percentage metal loading, more metal particles would remain within the fibers. However, it is also notable that the trend seems to suggest metal loadings of Fe and Ni actually lower surface area and pore volume of the support. In this respect, Co supported catalysts may yield the most promising product for further catalyst use (e.g. in fuel cell cathodes).

Table 2. BET Surface Area and BJH Desorption*

Catalytic Precursor	Treatment	BET Surface Area (m^2/g)	BJH Desorption (cm^3/g)
SiO_2	900ºC, 2 hours	288	.88
2% Co/SiO_2	900ºC, 2 hours	465	.92
5% Co/SiO_2	900ºC, 2 hours	248	.61
10% Co/SiO_2	900ºC, 2 hours	214	.44
2% Fe/SiO_2	900ºC, 2 hours	255	.62
2% Ni/SiO_2 **	900ºC, 2 hours	N/A	N/A
MgO	900ºC, 2 hours	181	.95
2% Co/MgO	900ºC, 2 hours	287	1.08
2% Fe/MgO	900ºC, 2 hours	218	.90
2% Ni/MgO	900ºC, 2 hours	128	.45
MgO(nanopowder)	900ºC, 2 hours	256	1.21
%Fe/MgO(nanopowder)	900ºC, 2 hours	241	1.20

* Note that samples prepared with the 550ºC, 4 hour treatment were not tested. The yield was low, and the fibers were used in other tests.
** Unforeseen circumstances caused this sample to be unavailable for this particular characterization testing.

4.3) Temperature Programmed Acetonitrile Pyrolysis (TPAP)

A small scaled version of the acetonitrile pyrolysis was carried out. Analysis of the byproducts produced from the different catalytic precursors was done using a Cirrus MS. Ions with an AMU between 1 and 100 were scanned with specific attention paid to the ions resulting from the decomposition of acetonitrile. The data obtained from the different catalytic precursors were nearly the same. By counting the ions, for each mole CH_3CN, approximately 0.56 mol HCN, 0.30 mol CH_4, 0.10 mol N_2 and 0.23 mol H_2 can be accounted for. Based on mole balances, the species not quantified or not detected by MS contain approximately 1.14 moles of C, 0.23 moles of N, and 0.80 moles of H. **(**See the appendix for further details of the calculation.) The undetectable species likely include tars and nitrogen-containing solid carbon. After a typical acetonitrile treatment, deposition of elemental carbon is apparent from the black color of the treated samples

and their increased mass, while brown tar can be seen near the exit of the furnace and in the exit stream water trap.

4.4) Temperature Programmed Oxidation (TPO)

TPO was used to analyze and determine the oxides of both nitrogen and carbon that formed from the combustion reaction of the samples. A Setaram TG-DSC 111 was used to monitor mass changes during the combustion, while a Cirrus Mass Spectrometer (MS) analyzed the product stream. The fibers that were analyzed were the washed samples prepared from acetonitrile pyrolysis at 900ºC for 2 hours. Trends for the nitrogen oxides and carbon oxides were recorded. A computer program then integrated the area under the curve, which was then used to determine the composition of the nanofibers that were grown. Table 3 summarizes the results of the TPO testing.

Table 3. Results of Oxidation Analysis

Support	Metal Loading	Wash Conditions	% of Mass Combusted	% N
SiO_2	None	KOH, HCl	61%	1.1%
SiO_2	2% Fe	KOH, HCl	83%	0.8%
SiO_2	2% Co	KOH, HCl	60%	2.9%
SiO_2	2% Co	HF	72%	2.9%
SiO_2	5% Co	KOH, HCl	83%	1.9%
SiO_2	10% Co	KOH, HCl	44%	2.1%
SiO_2	2% Ni	KOH, HCl	49%	1.5%
MgO	None	HCl	81%	1.6%
MgO	2% Fe	HCl	93%	0.9%
MgO	2% Co	HCl	86%	1.5%
MgO	2% Ni	HCl	90%	0.9%
MgO(nanopowder)	None	HCl	87%	1.4%

The percentage nitrogen in the resulting carbon nanofibers indicates to what degree the carbon fibers were doped. From Table 3, Co supported catalysts appear to have grown fibers with a higher percentage of nitrogen, when compared to catalysts with the same support. Additionally it is important to note that the percentage of mass combusted from fibers grown on the SiO_2 supported samples were a lot lower than that of MgO. The difference in combustion shows that more weight was left after combusting the fibers produced from the SiO_2 supported catalytic precursor, which suggests that more SiO_2 remained in the fibers even after fiber washing. This result, again, is another indication that the purification process for SiO_2 is not as effective as the one for MgO. (Recall Figure 6 and Figure 7 where washing of the MgO based sample seemed to open up the pores more than the washing of the SiO_2 based sample.)

4.5) Transmission Electron Microscopy (TEM)

TEM was the characterization method used to physically look at the samples. By examining the cross section of the nitrogen-containing carbon nanofibers grown, the fact that the nanoparticles are tubes was confirmed. Physical characteristics of the fibers grown from different catalytic precursors could be examined and categorized. Additionally, size distributions of the fibers as well as hypotheses of the fiber growth process can be made.

Figure 8 and Figure 9 show images of the growth produced from the SiO_2 catalyst, which was treated with acetonitrile at 900ºC. The TEM images were taken of samples that had already been purified. Figure 8 focuses on an overall view of the fibers grown from SiO_2, while Figure 9 shows a close up featuring two types of carbons that were grown: (1) amorphous carbon and (2) graphitic shells.

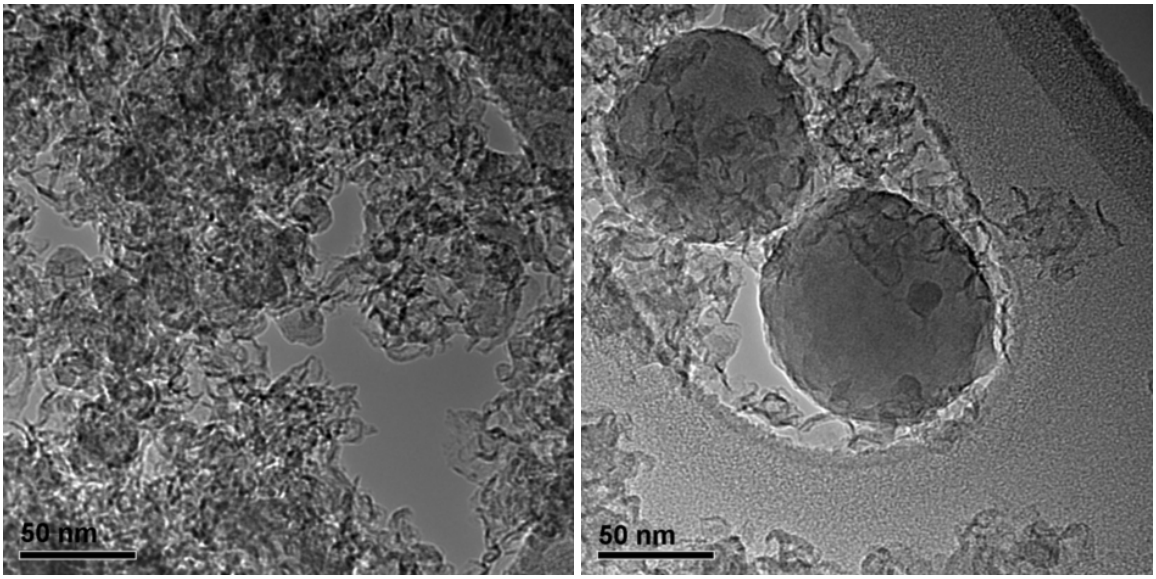

(a) (b)

Figure 8. TEM images of shells grown from acetonitrile pyrolysis over SiO_2 at 900ºC, post purification

(a) This shows the representative sampling of the shells grown.
(b) A close up of some of the different types of shells formed. Both graphite shells as well as amorphous carbon can be seen.

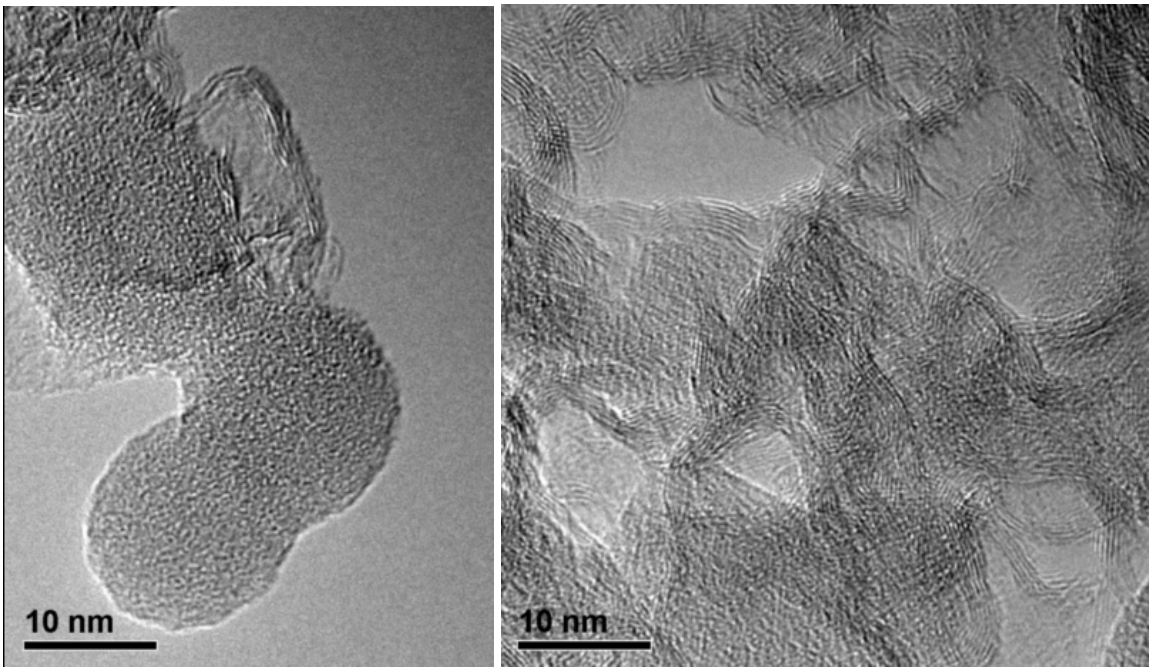

(a) (b)

Figure 9. TEM images of shells grown from acetonitrile pyrolysis over SiO_2 at 900ºC, post purification (zoomed in on different types of nanofibers grown).

(a) This an example of amorphous carbon. Note the lack of shape or graphite planes.
(b) The picture depicts shells showing some graphite planes.

Many different types of carbon are grown from the SiO_2 catalyst. From Figure 9a, it clear that amorphous carbon does not have the ordered sheets. Because of the lack of the ordered planes, amorphous carbon is not as useful for catalytic purposes. Figure 9b shows indications of shells with graphitic qualities. The shells can be labeled as such, because it is clear that they do have ordered planes.

The growth from the acetonitrile treatment over both MgO supports were also analyzed using TEM. Figure 10 shows the shells grown from the commercially bought MgO support, and Figure 11 depicts images of the shells obtained from treatment of the MgO nanopowder support.

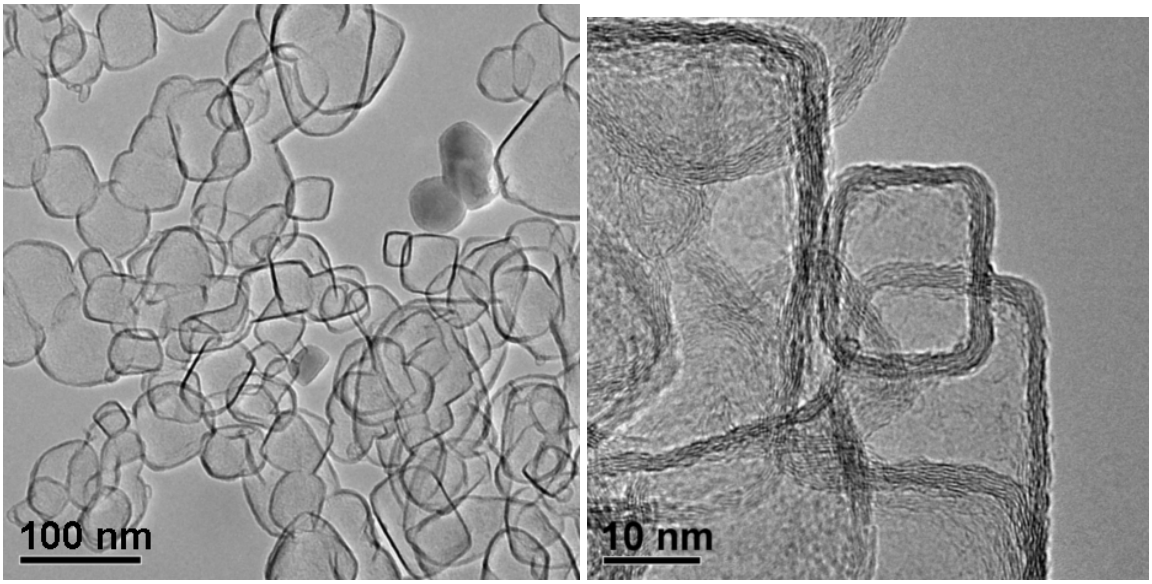

(a) (b)

Figure 10. TEM images of shells grown from acetonitrile pyrolysis over MgO, post purification.

(a) Zoomed out version of the type of the shells that are grown from the MgO catalyst.
(b) Zoomed in version of the type of the shells that are grown from the MgO catalyst.

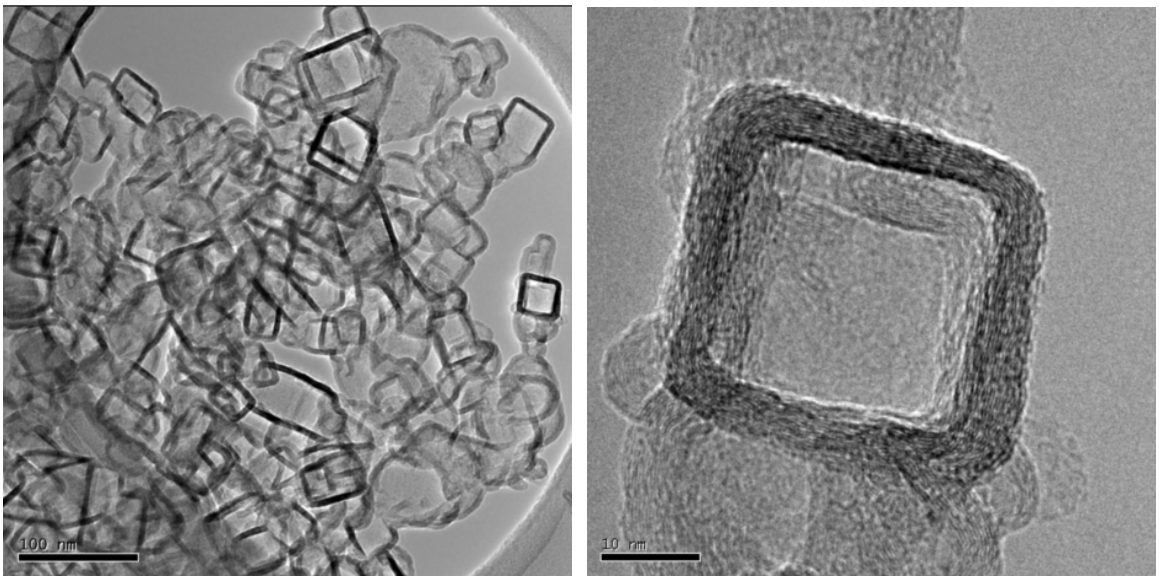

Figure 11. TEM images of shells grown from acetonitrile pyrolysis over MgO nanopowder, post purification.

(a) Zoomed out version of the type of shells that are grown from the MgO nanopowder catalyst.
(b) Zoomed in version of the type of shells that are grown from the MgO nanopowder catalyst.

The nanostructures of the fibers grown from both of the MgO catalytic precursors are much different than those produced from SiO_2 (Figure 8, Figure 9). From Figure 10a and Figure 11a, it is apparent that not much amorphous carbon exists. Instead, the graphitic shells mostly seem to have aligned planes which have formed into a boxy shape, which can be attributed to the crystalline shape of MgO particles. This hypothesis can be confirmed in the subsequent zoomed in pictures, Figure 10b and Figure 11b. In a TEM image, blank air is represented by a uniform gray color. However, within the boxy structures, the coloring is not uniformly gray. Instead, it has a speckled image, which indicates that something, in this case the MgO support, had once filled the area.

By comparing the different MgO supports, subtle differences can be observed. For the most part, the box-like structures of the shells grown from the MgO nanopowder seemed to be smaller in area, which can be attributed to the fact that the particles of the nanopowder were smaller than that of the normal MgO. Additionally, the graphitic shells grown around the nanopowder was thicker as well. Again, this observed phenomena can probably be attributed to the physical differences between the two MgO supports tested. Perhaps the larger pore volume and the fluffier texture allowed the fibers to grow more unrestrictedly. Although these small differences were detected, the morphology of the graphitic shells produced was not significantly different between the MgO and MgO (nanopowder) supports; however, the shells grown from pure SiO_2 had were different in shape from those grown from the MgO support.

After basic shapes of the shells that were grown from the pure supports were identified, the products, which in this case are carbon nanofibers, of acetonitrile treated metal supported catalysts were also analyzed. The affect of metal on the fibers produced can then be seen, and additional comments about the nanostructures and growth process over the metals can be made. Figure 12 shows the images of different metal loadings on the SiO_2 support. Figure 13 depicts the data retrieved from TEM analysis of different metal loadings over the MgO support.

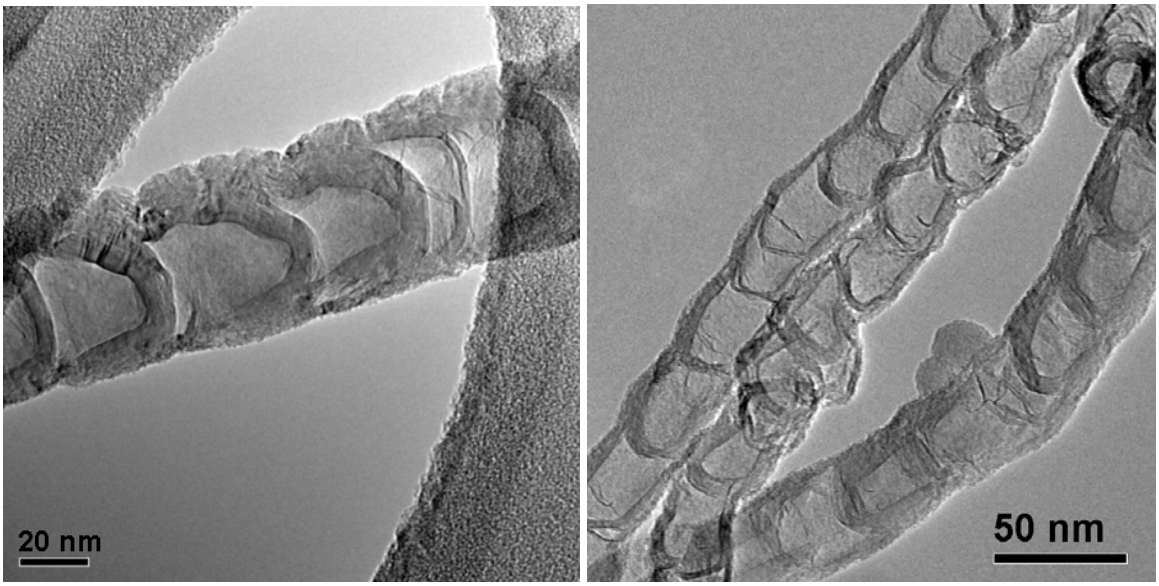

(a) (b)

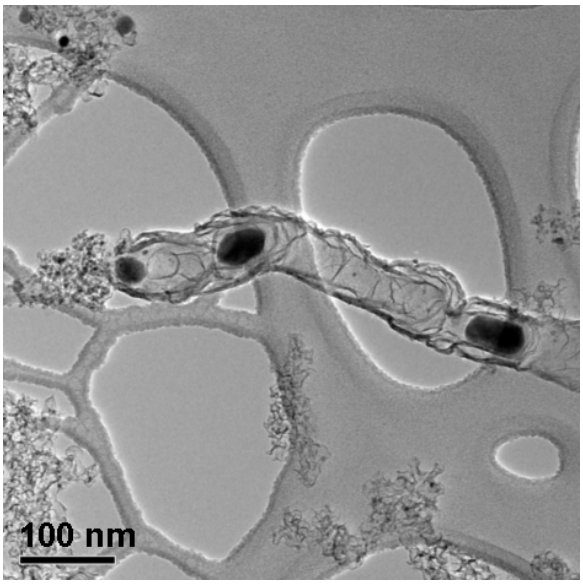

(c)

Figure 12: TEM images of fibers grown from acetonitrile pyrolysis over different metals loaded on SiO_2 at 900ºC, post purification

(a) Fibers grown from 2% Fe/SiO_2
(b) Fibers grown from 2% Co/SiO_2
(c) Fibers grown from 2% Ni/SiO_2

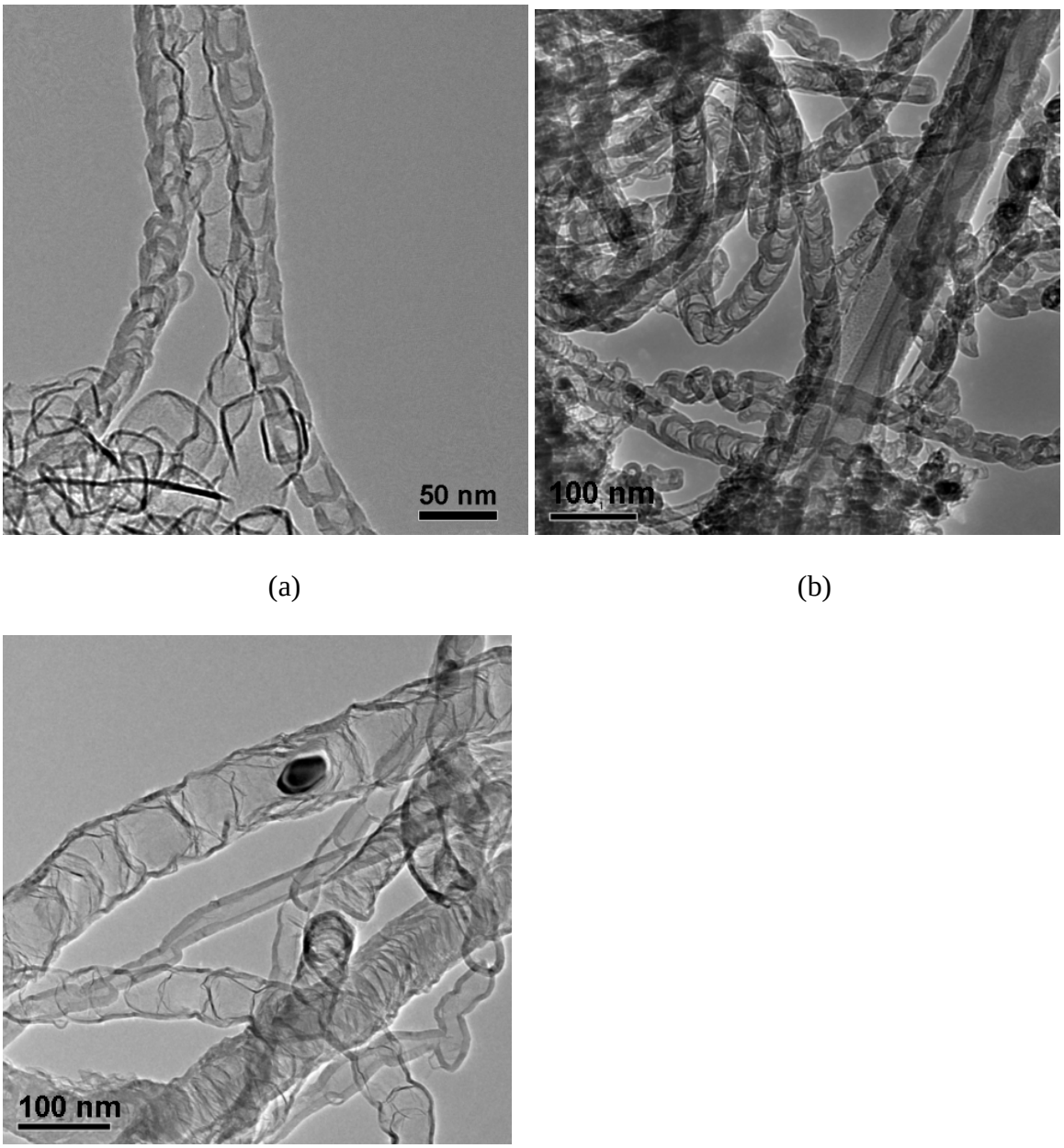

(a) (b)

(c)

Figure 13: TEM images of fibers grown from acetonitrile pyrolysis over different metals loaded on MgO, post purification

(a) Fibers grown from 2% Fe/MgO
(b) Fibers grown from 2% Co/MgO
(c) Fibers grown from 2% Ni/MgO

Figure 12 explores the different types of fibers grown form the acetonitrile pyrolysis of SiO_2 metal catalysts. From the images, the 2% Fe/SiO_2 catalyst precursor yielded fibers that were of a stacked cup shape (Figure 12a). Figure 12b shows that the 2% Co/SiO_2 catalyst precursor resulted in fibers with nearly the same structure as well. A clear difference can be seen, however. The fibers grown from the Fe are much thicker than those that are grown from Co. Additionally, these cup shapes are seen to be completely compartmentalized. The structure is a cross between the MWNTs and stacked platelet carbon depicted in Figure 1 and Figure 2, respectively, which could give this type of carbon nanofiber the properties of both activity and conductivity. The 2% Ni/SiO_2 catalytic precursor grew fibers that were differently structured than the other two metal loadings. This result can be seen visually with Figure 12c. The fibers seen are in a sort of broken ladder shape. Instead of being compartmentalized like the stacked cups, they seem to have grown perpendicularly to the fiber axis only. It is also important to note that metal chunks are trapped within the ladders; however, the fibers did not give an indication to having a propensity to grow perpendicular to the fiber axis.

Similarly to Figure 12, Figure 13 depicts the different types of carbon nanofibers grown from the metal catalysts supported by MgO, post acetonitrile treatment. Similar trends were seen. In Figure 13a and Figure 13b, the stacked cup nanostructure clearly prevailed. Therefore, Fe and Co seem to grow the same shaped fibers regardless of the support. Again, the fibers grown from Fe seem thicker than those grown from Co. Additionally, the fibers grown from 2% Ni/MgO and 2% Ni/SiO_2 are similar as well. Again, the carbon fibers have a broken ladder structure with entrapped metal particles.

From the observed samples, four different types of nanofibers were observed. Stacked cups, MWNTs, and ladders have already been previously mentioned. A fourth type was discovered, and it is denoted as a solid fiber (shown in Figure 14). By looking at a sampling of the different samples, a breakdown of the type of fibers grown could be made as well. See Table 4 for the reported results.

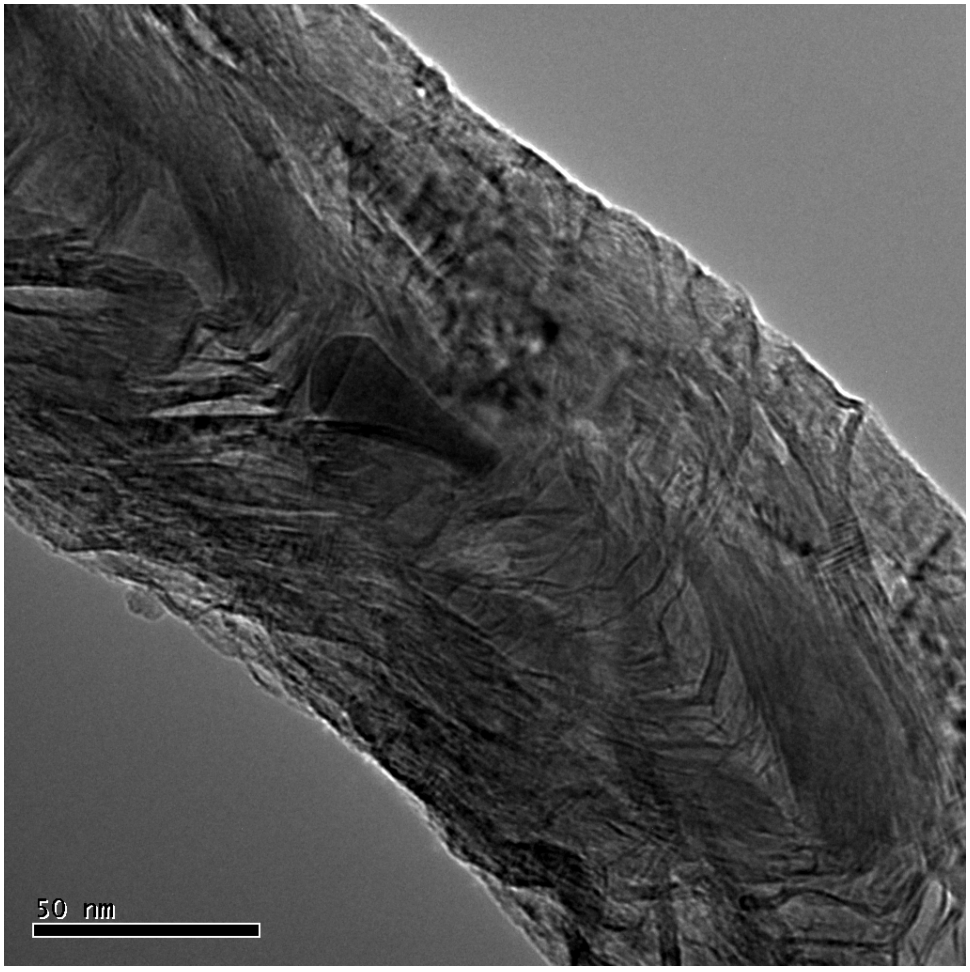

Figure 14. Solid Fibers grown from acetonitrile pyrolysis over 2% Fe/SiO_2

Table 4. Breakdown of different types of nanofibers found

Catalytic Precursor	Stacked Cups	Solid Fibers	MWNTs	Ladders
2% Co/SiO_2	66%	0%	13%	21%
2% Fe/SiO_2	71%	7%	18%	4%
2% Ni/SiO_2 *	N/A	N/A	N/A	N/A
2% Co/MgO	54%	10%	21%	15%
2% Fe/MgO	42%	14%	9%	35%
2% Ni/MgO	13%	25%	18%	45%
%Fe/MgO(nanopowder)	60%	10%	20%	10%

* Unforeseen circumstances caused this sample to be unavailable for this particular characterization testing.

The stacked cup structured nanofibers are most useful for catalytic activity, while MWNTs seem to have the most use for conductivity as well as mechanical reinforcements. Because of those reasons, these two types of fibers should be looked upon more favorably, depending on which function is needed from the nanofibers. Following the trends in Table 4, samples with Co and Fe yielded a much higher percentage of the stacked cup structure than the Ni samples. As seen in Figure 13, the 2% Ni/MgO catalytic precursor yielded fibers with mostly the broken ladder form (assuming the same result would have been found if the 2% Ni/SiO_2 sample could have been analyzed).

TEM was not only employed in order to analyze the structures of the nanofibers, but it was also used to determine the sizes of the fibers produced from different catalytic precursors. By taking sample measurements of fiber diameters of the different catalytic precursors, comparisons of the affect of catalytic precursor on fiber size can be made. A sampling size of approximately 50 different measurements was made. Figure 15 and Figure 16 depict fiber diameters obtained from SiO_2 supported catalysts and MgO (regular and nanopowder, which is denoted by HSA, high surface area), respectively.

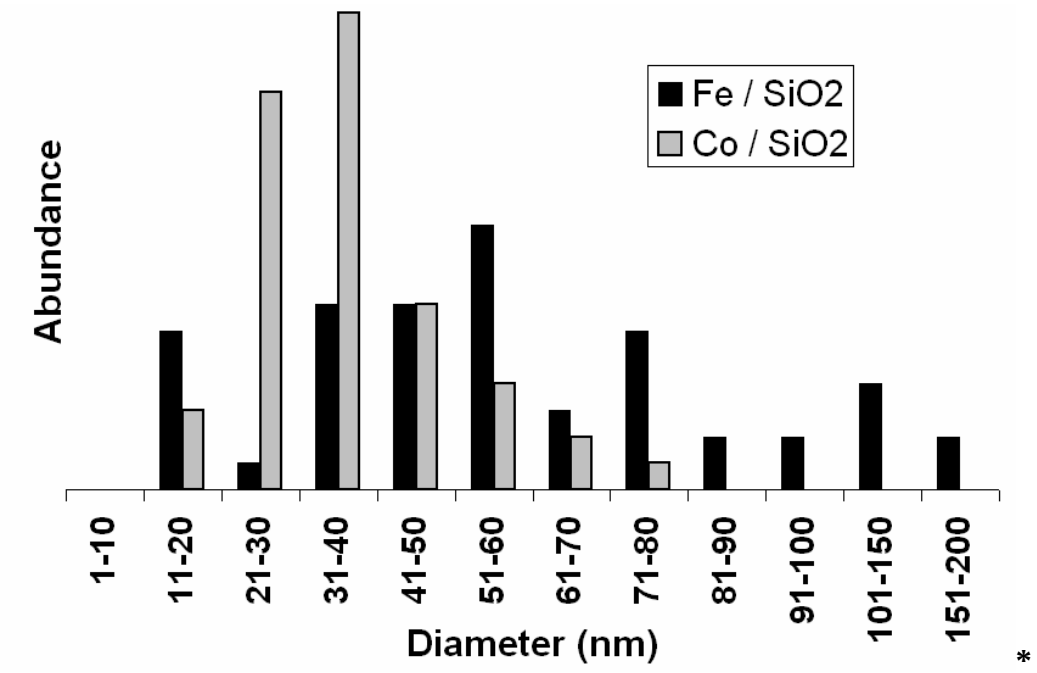

Figure 15. Diameter distribution of fibers produced from SiO_2 supports

* Analysis for the Ni/SiO_2 sample could not be done, because there were not many fibers in it.

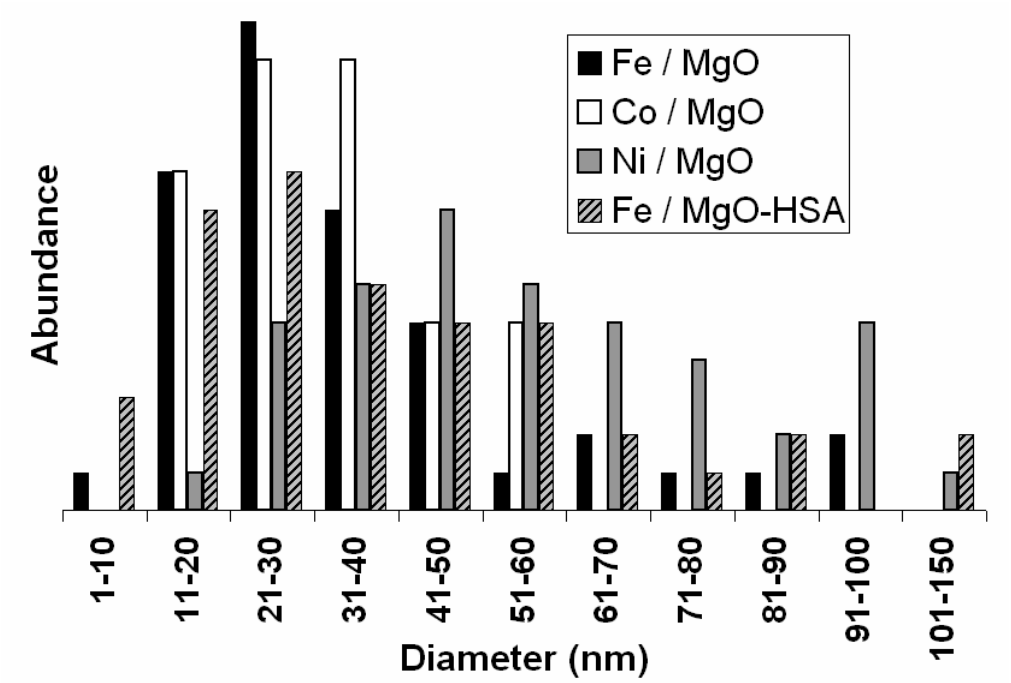

Figure 16. Diameter distribution of fibers produced from MgO supports

Figure 15 shows that on the SiO_2 supported catalysts, the fibers grown range from 11 nm to 200 nm. With this particular support, the Fe sample produced nanofibers that peaked in the 51 - 60 nm range for the diameter. However, the spread for the Fe/SiO_2 sample had a much more even spread than the Co/SiO_2 sample. The Co impregnated SiO_2 sample peaked at an earlier diameter range, 31 – 40 nm with an notable amount being in the 21 – 30 nm range as well. This distribution, however tapers off, showing that no fibers were found yielding a diameter over 80 nm. Measured diameter data for the fibers grown on MgO supported catalysts are found in Figure 16. A qualitative comparison shows that the fibers grown from the Ni/MgO catalyst had a relatively large size distribution, with nearly an equal spread of fibers amongst the distribution. Even with that specific trend seen, that particular catalytic precursor still yielded fibers with a nearly Gaussian distribution of diameters, which occurred within the 41 – 50 nm range. The fibers produced via the Co/MgO catalyst had approximately the same distribution as the ones produced via the Co/SiO_2 catalyst. The range that included most of the diameters spread was between 21 – 40 nm. On MgO, the Fe sample produced fibers that were even smaller than the SiO_2 supported counterpart. Both Fe/MgO and Fe/MgO (nanopowder) produced fibers whose diameter mostly fell between 11 – 50 nm. In addition to having the fibers be smaller, the range of the diameters produced from catalyst with the MgO support was significantly smaller as well. By knowing the size distributions of fibers created, a process can be tailored in order to produce nitrogen containing nanofibers at the size needed for different usages.

In addition to being able to give us information about fiber shapes and size distribution, TEM images can also help lead to other conclusions as well. By looking at

the pictures, hypotheses about the process in which fibers are grown can be made. Using fibers produced from pyrolysis over the 2% Fe/MgO catalytic precursors as an example can help with drawing such conclusions, as shown in Figure 17 and Figure 18.

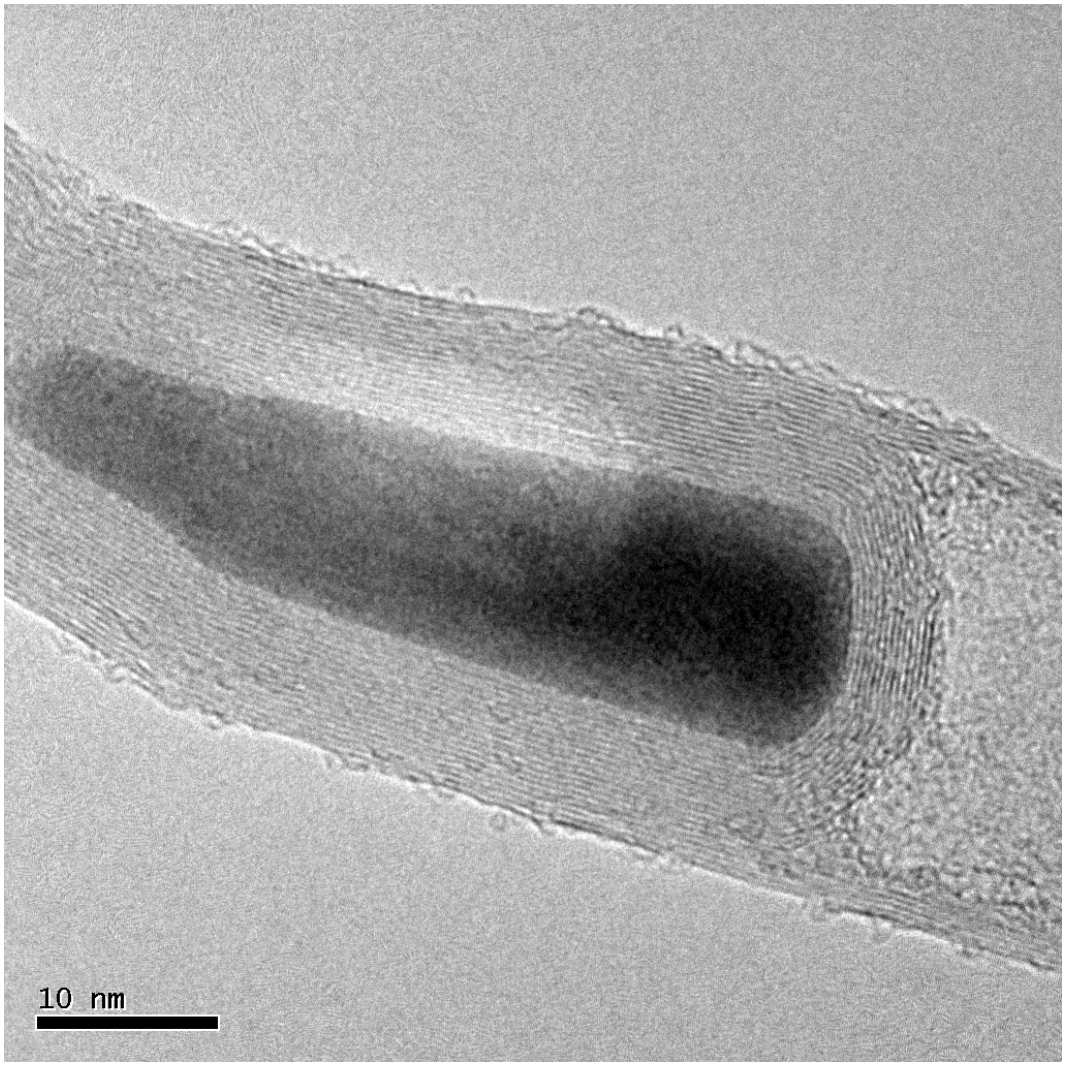

Figure 17. Close up picture of Fe trapped in nanofibers grown from acetonitrile pyrolysis over a 2% Fe/MgO catalytic precursor.

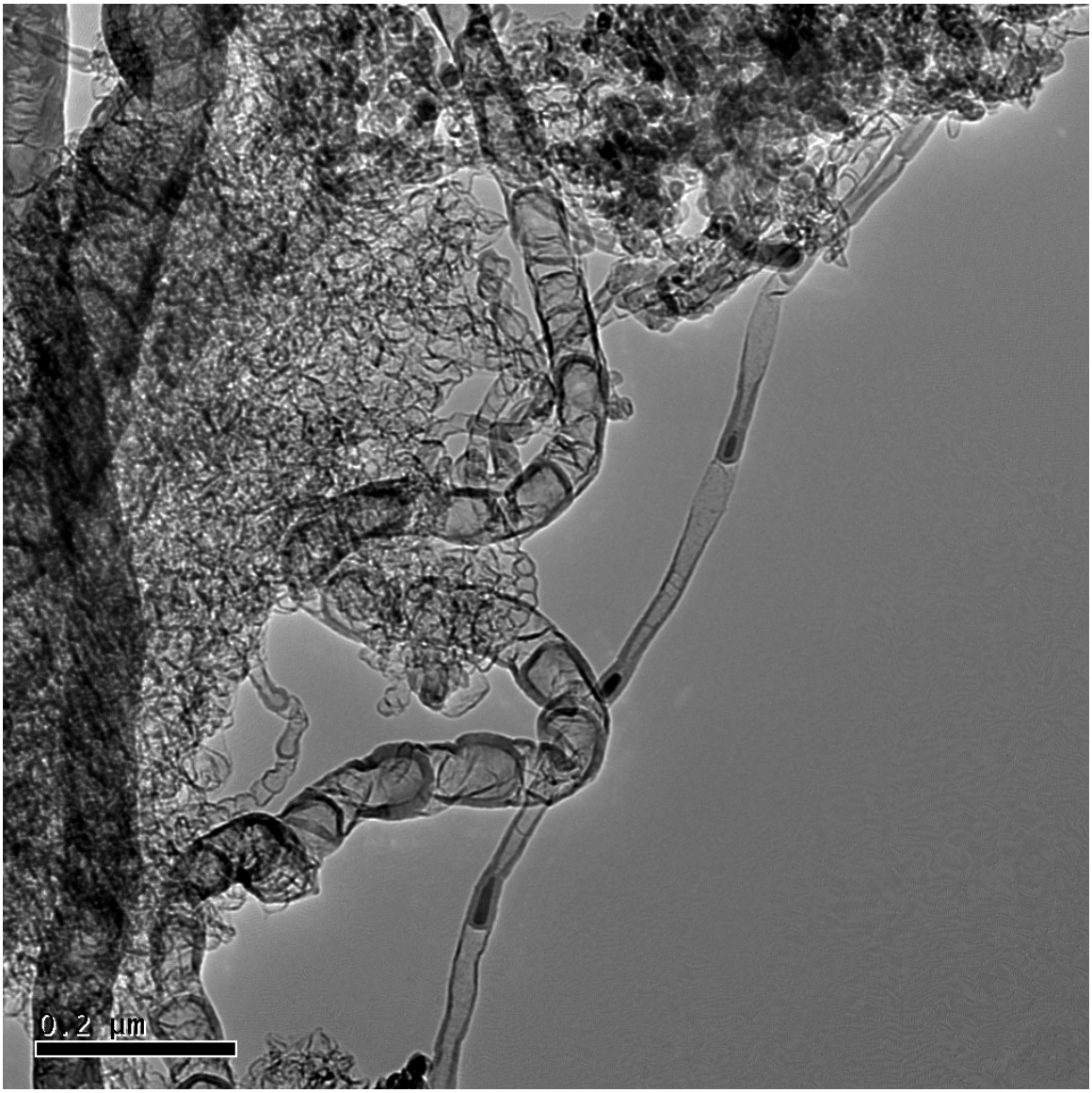

Figure 18. Picture of Fe trapped in nanofibers grown from acetonitrile pyrolysis over a 2% Fe/MgO catalytic precursor.

From Table 4, it was seen a majority of the nanofibers grown from 2% Fe/MgO were of the stacked cup structure (depicted in Figure 14a). However, Figure 17 shows a piece of Fe trapped in carbon nanofibers. This image shows that carbon nanofibers are grown from the metal particle. A zoomed out version, Figure 18, shows the stacked cup fibers with metals dispersed almost with approximate spatial uniformity throughout the fiber length. These images help with putting together a hypothesis on how fibers grow in this atmosphere. As previously noted, the fibers are grown on the surface of the metal particles. The stacked cup structure indicates that the metal is pushed upwards with the growth. Figure 18, however, indicates that the metal may have broken into pieces at some point in order to give us the observed pattern. Given the TEM images, the hypothesis made is a reasonable one for explaining the behavior of fiber growth in the acetonitrile decomposition process.

5) Summary

Nitrogen-containing nanofibers are lightweight and can be functionalized for electrical and thermal conductivity. Additionally, it has the potential to be used in mechanical reinforcement. Because of the aforementioned properties, they have the potential to be used in many applications including fuel cell cathodes, water purification systems, and nanoelectronics. However, different metals and supports change the growth atmosphere, and thus the carbon nanofiber structure.

Figure 5 summarizes the catalyst preparation and testing process. Different combinations of metals and supports were created. From that point, the vertical proceedings represent the preparation of the fibers. These steps included using incipient wetness to create the catalytic precursor, subjecting the catalyst to acetonitrile decomposition, and finally purifying the fibers. The horizontal arrows branching out from different steps indicate the different characterization tests that were completed at that stage. These tests included BET surface area/pore volume analysis, TGA, TPAP, TEM, and TPO.

The goal of exploring new means of fiber preparation was to get a higher yield of fibers that were easier to purify than previous methods. MgO supports seem like a better choice than the SiO_2 supports, since BET surface area/pore volume testing showed that purifying MgO was more effective. Additionally, TPO data showed that less mass percentage combusted from the SiO_2 prepared fibers, another indication that the support was left in the sample after purification. In order to identify the amount of nitrogen in the fibers, TPO data was helpful. Co doped catalysts generally produced fibers with a higher nitrogen content. After TGA was taken into account, both Co and Fe catalysts grew a

significant amount of fibers, while Ni containing catalysts did not. TEM helped analyze fiber shape and size distribution. Stacked cup forms, available in large quantities from Co and Fe doped catalytic precursors, are good for catalytic activity because of exposed edge planes. Again, size distribution did not vary much with the different support. However, Co doped catalysts produced fibers with more uniformity. By analyzing different growth atmospheres and their affects on nitrogen-containing carbon nanofibers has helped to tailor these fibers with respect to shape, size, and nitrogen content depending on what characteristics are needed.

Bibliography

[1] Park, C., Keane, M.A., "Catalyst support effects in the growth of structured carbon from the decomposition of ethylene over nickel," *Journal of Catalysis.* **221** (2004) 386.

[2] Anderson, P.E., Rodriguez, N.M., "Influence of the Support on the Structural Characteristics of Carbon Nanofibers Produced from the Metal-Catalyzed Decomposition of Ethylene," *Chem. Mater.* **12** (2000) 823.

[3] Matter, P.H., Zhang, L., Ozkan, U.S., "The role of nanostructure in nitrogen-containing carbon catalysts for the oxygen reduction reaction," *Journal of Catalysis.* **239** (2006) 83.

[4] Rodriguez, N.M., Chambers, A., Baker R.T.K., "Catalytic Engineering of Carbon Nanostructures," *Langmuir*. **11** (1995) 3862.

[5] Maldonado, S., Stevenson, K.J., "Influence of Nitrogen Doping on Oxygen Reduction Electrocatalysis at Carbon Nanofiber Electrodes," *J. Phys. Chem. B.* **109** (2004) 4704.

[6] Singh, C., Quested, T., Boothroyd, C.B., Thomas, P., Kinloch, I.Z., Abou-Kandil, A.I., and Windle, A.H., "Synthesis and Characterization of Carbon Nanofibers Produced by the Floating Catalyst method," *J. Phys. Chem B.* **106** (2002) 10915.

[7] Park, C., Engel, E.S., Crowe, A., Gilbert, T.R., Rodriguez, N.M., "Use of Carbon Nanofibers in the Removal of Organic Solvents from Water," *Langmuir*. **16** (2000) 8050.

[8] Huang, Y., Gao, J. Liu, R., "Structure and electronic properties of nitrogen-containing carbon nanotubes,"*Synthetic Metals*. **113** (2000) 251.

[9] Gonzalez, R.D., Lopez, T., Gomez, Ricardo., "Sol-Gel preparation of supported metal catalysts," *Catalysis Today*. **35** (1997) 293.

[10] von Dommele, S., Romero-Izquirdo, A., de Jong, K.P., Bitter, J.H., "Nitrogen-Containing Carbon Nanotubes as Solid Base Catalysts," *Proceedings of the 19th NACS Meeting,* Philadelphia, PA, 2005.

[11] Kirk and Othmer Encyclopedia of Chemical Technology, "Carbon Fiber Manufacturing Processes – Polyacrylonitrile Carbon Fiber Process," *Carbon and Graphite Fibers.* **5** (1991) 5.

[12] Gupta, S., Tryk, D., Bae, I., Aldred, W., Yeager, E., "Heat-treated polyacrylonitrile-based catalyst for oxygen electroreduction," *Journal of Applied Electrochem.* (1989) 19.

[13] Biniak, S., Walczyk, M., Szymanski, G.S., "Modified porous carbon materials as catalytic support for cathodic reduction of dioxygen," *Fuel Processing Technology*. **79** (2002) 251.

Appendix

Appendix 1: Setup of the system used for the acetonitrile pyrolysis treatment.

Appendix 2: Sample calculation using TPAP data to analyze byproducts of the acetonitrile pyrolysis treatment.

Appendix 1: Setup of the system used for the acetonitrile pyrolysis treatment.

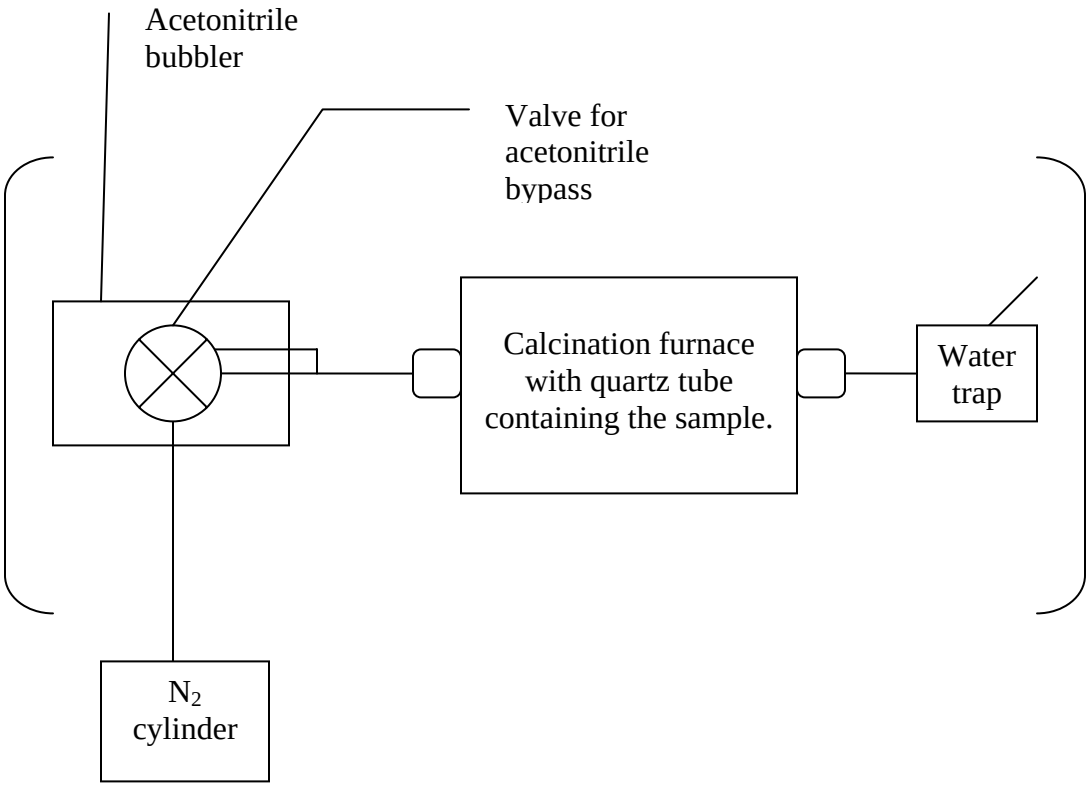

Note:
"[ ]" denotes the parts of the process that are carried out under a fume hood.

A tube clamp to make sure acetonitrile did not leak into the quartz tube when the bypass was closed was in the set up. However is not shown in the diagram.

Figure 19. Setup of the system used for the acetonitrile pyrolysis treatment.

Appendix 2: Sample calculation using TPAP data to analyze byproducts of the acetonitrile pyrolysis treatment.

Table 5 shows the initial amount of acetonitrile found before the decomposition took effect. Table 6 shows the ions accounted for at the final temperature of the temperature ramp (900ºC). The data used was from the data obtained by the MS.

Table 5. Fe/SiO_2 at T = 500ºC

ion	Abundance	Species	Total Abundance	Estimated Flow (sccm)	H out	N out	C out
42	0.0993	CH_3CN	4.03	2.00	6.00	2.00	4.00
41	1.69	"					
40	1.22	"					
39	0.66	"					
38	0.37	"					

Table 6. Fe/SiO_2 at T = 900ºC

ion	Abundance	Species	Total Abundance	Estimated Flow (sccm)	H out	N out	C out
27	1.37	HCN	1.72	0.85	0.85	0.85	0.85
26	0.35	HCN					
16	0.88	CH_4	1.72	0.85	3.40	0.00	0.85
15	0.69	CH_4					
14	0.15	CH_4					
2	0.85	H_2	0.85	0.42	0.84	0.00	0.00
28	0.76	N_2	0.76	0.37	0.00	0.75	0.00
			Totals =	2.50	5.10	1.60	1.71
				% =	85%	80%	43%

To get a 1 mol basis, divide all of the total abundance values in Table 6 by the CH_3CN total abundance found in Table 5.

Ex: Take N_2 as the species in question.

$$\frac{TotAb_{N2}}{TotAb_{CH3CN}} = \frac{.76\_molN_2}{4.03\_molCH_3CN} = .19\frac{molN_2}{molCH_3CN}$$

Using molar relations, the amount of each element in acetonitrile (H, C, and N) were calculated in conjunction with the estimated volumetric flowrate. This calculation was completed for both the initial temperature (500ºC) and the final temperature (900ºC). At the final temperature, acetonitrile had decomposed, and the important species taken into account were HCN, CH_4, H_2, and N_2. The percent recovery of each element could then be subsequently calculated for. See the example below.

Ex: Take N into account.

At T = 500ºC

$$2.00\_sccmCH_3CN * \frac{1\_molN}{1\_molCH_3CN} = 2\_sccmN_{out}$$

The same process was followed with the species that contained N at T=900ºC.

After N_{out} was calculated for HCN and N_2, total N_{out} was calculated.

In this case N_{out} = 1.60 sccm N_{out}.

The percentage recovered was then tabulated:

$$\%N_2 recovered = \frac{N_{out\_final}}{N_{out\_initial}} * 100\% = \frac{1.60}{2.00} * 100\% = 80\%$$

From that, the mole amount of N unaccounted for could be calculated (with respect to a one molar basis of CH_3CN).

$$unaccounted\_N_2 = (100\% - \%N_2 recovered) * \frac{1\_molN}{1\_molCH_3CN} = (100\% - 80\%) * 1 = .2\_molN_2$$

This analysis was done on all of the samples; the results were then compared. Since they yielded similar numbers, an approximation was reported in the section 4.3.